VIP | **Protein Function** | *Very Important Paper*
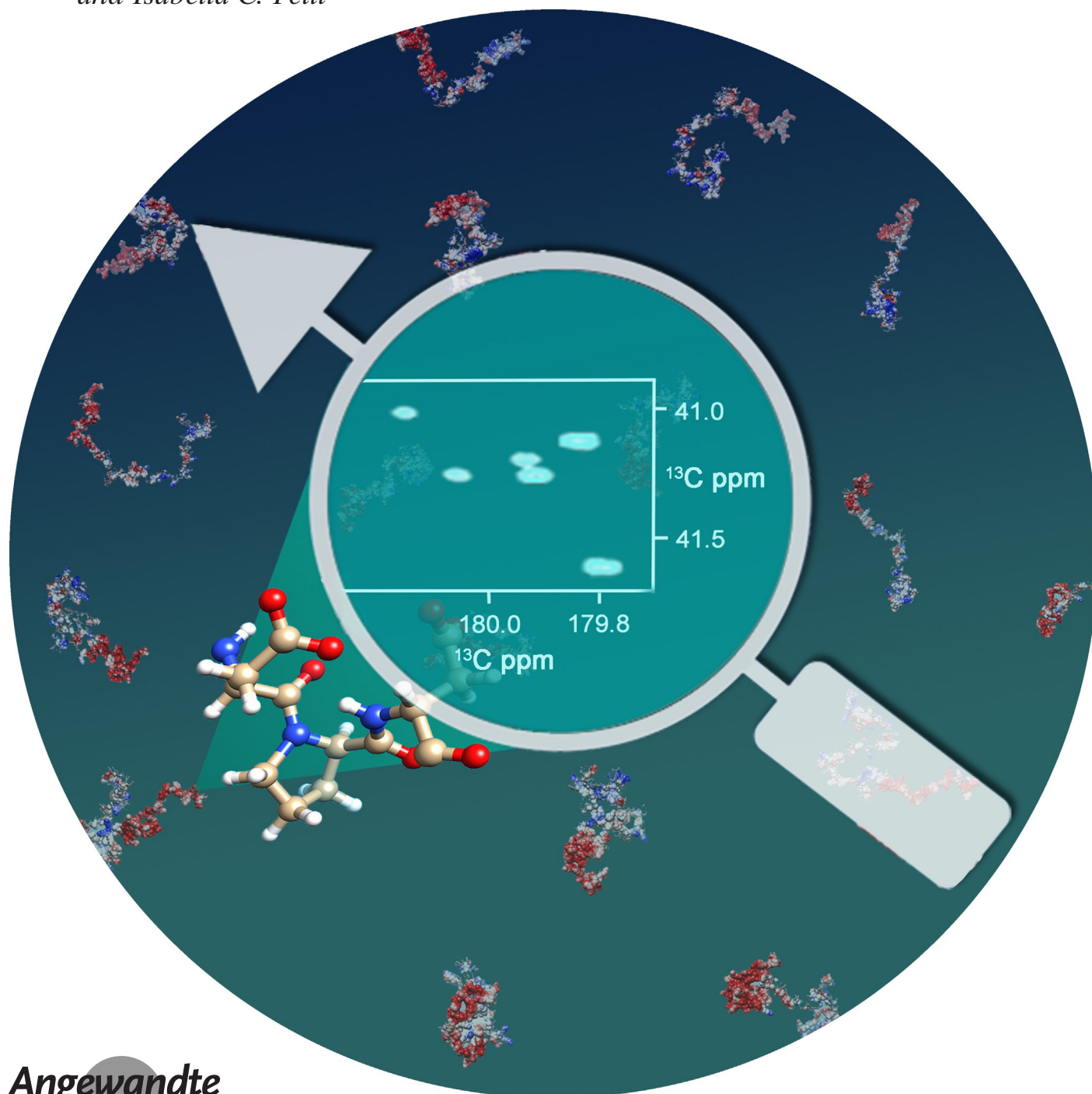
Monitoring the Interaction of α-Synuclein with Calcium Ions through Exclusively Heteronuclear Nuclear Magnetic Resonance Experiments

Letizia Pontoriero[+], Marco Schiavina[+], Maria Grazia Murrali, Roberta Pierattelli,* and Isabella C. Felli*

Abstract: Many properties of intrinsically disordered proteins (IDPs), or protein regions (IDRs), are modulated by the nature of amino acid side chains as well as by local solvent exposure. We propose a set of exclusively heteronuclear NMR experiments to investigate these features in different experimental conditions that are relevant for physiological function. The proposed approach is generally applicable to many IDPs/IDRs whose assignment is available in the Biological Magnetic Resonance Bank (BMRB) to investigate how their properties are modulated by different, physiologically relevant conditions. The experiments, tested on α-synuclein, are then used to investigate how α-synuclein senses Ca^{2+} concentration jumps associated with the transmission of nerve signals. Novel modules in the primary sequence of α-synuclein optimized for calcium sensing in highly flexible, disordered protein segments are identified.

Introduction

Intrinsically disordered proteins (IDPs) and protein regions (IDRs), which challenge the canonic structure-function paradigm, represent an emerging field of research in modern protein chemistry.[1–4] Highly flexible proteins and flexible linkers of complex proteins are present in any living organism and play key roles in a variety of different cellular pathways. They lack a stable three-dimensional structure in their native conditions while retaining biological activity. Initially described using creative epithets such as "dancing proteins", "protein clouds", "protein chameleons"[1] they are now widely investigated revealing novel ways through which extensive disorder and flexibility modulate protein function.

The structural and dynamic properties of IDPs/IDRs are even more influenced by the environment with respect to those of globular proteins.[5,6] Therefore experimental tools to study them in physiologically relevant conditions, all the way to in-cell, are very useful to understand the physicochemical properties relevant for their function and misfunction. In this framework, NMR spectroscopy provides a unique investigation tool to access high resolution information.[7,8]

Human α-synuclein is one of the most widely studied IDPs because of its involvement in several human neurodegenerative pathologies called synucleinopathies, such as Parkinson's disease (PD). Constituted by 140 amino acids, α-synuclein is intrinsically disordered in native conditions.

The primary sequence is generally subdivided into three different regions: the N-terminus (1–60), with several KTKXGV recognition motifs responsible for a net positive charge, the central, more hydrophobic, non-amyloid-β component NAC (61–94) and the C-terminal tail (95–140), a characteristic domain that is dense of negatively charged residues. Largely disordered in the monomeric state,[9] stabilized by long range interactions between the N-terminal region and the C-terminal region,[10,11] it adopts helical conformations when interacting with membranes through the N-terminal region[12–15] and elongated conformations in amyloid fibrils,[16] just to name a few snapshots on the most studied, heterogeneous structural properties of α-synuclein in different conditions.[17] In recent years many in vitro and in vivo studies were carried out to clarify the events that lead to the insurgence of different pathologies but the structural and dynamical versatility to different local conditions encountered in neuronal cells makes it difficult to identify those factors that trigger the pathological action of the protein as the formation of toxic aggregates. Full comprehension of the pathological and physiological roles of this biomolecule is still lacking in part because of the incredible range of environment-dependent conformational plasticity, a true "chameleon protein",[18] that renders its investigation very challenging.

Here we would like to present a novel set of 2D NMR experiments to follow how the properties of IDPs/IDRs change in different, physiologically relevant, experimental conditions. Based on carbonyl carbon direct detection,[19–25] these experiments provide information on backbone and side-chain chemical shifts as well as on the impact of solvent exchange at the residue level, even for those residues whose amide proton is not directly detectable. This set of 2D exclusively heteronuclear NMR experiments is tested on α-synuclein and then used to focus on its interaction with Ca^{2+}, a potential trigger for the onset of Parkinson's disease. Mainly localized in presynaptic terminals, α-synuclein is exposed to microdomains of high Ca^{2+} concentration associated with neurotransmitter release[26,27] and could be exposed to high extracellular Ca^{2+} concentration in cell-to-cell secretion mechanisms.[28] New insights on how a structurally and dynamically heterogeneous protein linked to the onset of Parkinson's disease senses these Ca^{2+} concentration jumps become thus very relevant to describe α-synuclein function.

Results and Discussion

Fingerprint of an IDP at physiological pH and temperature

The side chains of amino acids are seldom studied for IDPs/IDRs, even if they are expected to play important roles for their function because the extensive resonance overlap typical of their NMR spectra becomes even more pronounced when moving away from the backbone. 2D ^1H-^{13}C correlation spectra, even if highly sensitive, only show a small fraction of resolved cross-peaks, drastically reducing their high resolution information content. Carbon-13 detected 2D NMR experiments provide a valuable source of information. A

[*] L. Pontoriero,[+] M. Schiavina,[+] Dr. M. G. Murrali, Prof. R. Pierattelli, Prof. I. C. Felli
CERM and Department of Chemistry "Ugo Schiff"
University of Florence
Via Luigi Sacconi 6, 50019 Sesto Fiorentino, Florence (Italy)
E-mail: roberta.pierattelli@unifi.it
        felli@cerm.unifi.it

Dr. M. G. Murrali
Present address: Department of Chemistry and Biochemistry
University of California at Los Angeles (USA)

[+] These authors contributed equally to this work.

Supporting information and the ORCID identification number(s) for the author(s) of this article can be found under:
https://doi.org/10.1002/anie.202008079.

fingerprint of an IDP/IDR at physiological pH and temperature can be obtained through the set of 2D exclusively heteronuclear NMR experiments based on carbonyl carbon direct detection (CON, CACO, CBCACO, and CCCO).[29,30] However, extremely high resolution is needed to resolve resonances of side chains which cluster in very narrow spectral regions. To this end CACO, CBCACO, and CCCO pulse sequences were modified to achieve the necessary resolution to study IDPs/IDRs (Supporting Information, Figure S1); experimental variants exploiting ^{1}H polarization as a starting source (^{1}H-start) were also implemented to increase the sensitivity of the experiments (Figure S2).

Carbon-13 detected 2D NMR experiments reveal atomic resolution information for aliphatic as well as for carbonyl/carboxylate resonances of amino acid side chains (-COO$^-$, -CONH$_2$). As an example of the quality of the spectra that can be obtained, the assignment of the resonances of the six aspartate residues present in α-synuclein is shown in Figure 1. As illustrated for Asp 2, starting from the backbone carbonyl (C'_i) identified through the CON (C'_i-N_{i+1}), the resonances of C^α_i and C^β_i can be easily identified through inspection of the CACO and CBCACO. These are also correlated to the side-chain carboxylate carbon resonance (C^γ_i) through two additional cross-peaks in a close but well isolated spectral region. Therefore, the C^β_i-C^γ_i cross-peaks of the six aspartate residues can be easily assigned in a sequence-specific manner. Analogously, also asparagine side-chain resonances can be assigned. For glutamate and glutamine residues inspection of CCCO is also needed to unambiguously correlate the backbone carbonyl resonance to the C^α_i, C^β_i, C^γ_i aliphatic side-chain resonances and finally to the C^δ_i carbonyl/carboxylate resonances. The cross-peaks assignment of the carboxylate/carbonyl functional groups for α-synuclein (C^β_i-C^γ_i for Asp and Asn, C^γ_i-C^δ_i for Glu and Gln), which fall in a very clean spectral region, is reported in Table S2 (Supporting Information).

It is worth noting that carbonyl/carboxylate side-chain resonances are seldom assigned, in particular for IDPs/IDRs. They can be detected through triple resonance experiments based on amide proton detection.[31–33] However this approach is bound to fail in conditions in which amide protons are not detectable, such as for solvent-exposed protein backbones at physiological pH and temperature. 2D exclusively heteronuclear NMR experiments enable us to easily assign side-chain resonances, starting from the backbone assignment, adjusting chemical shifts to the conditions under investigation through inspection of a CON spectrum, followed by the analysis of the CACO/CBCACO/CCCO spectra. This constitutes a general approach to access additional key information for any IDP/IDR whose assignment is available in the Biological Magnetic Resonance Bank (BMRB, http://www.bmrb.wisc.edu/). This set of spectra thus provides a unique tool to achieve a fingerprint of an IDP near physiological conditions not only for backbone resonances but also for side chains.

Negatively charged side chains of aspartate and glutamate residues are the first candidates to establish interactions with oppositely charged polypeptide chains[34] as well as to interact with metal ions.[35–39] Particularly relevant for α-synuclein function is the interaction with Ca^{2+} involved in the trans-
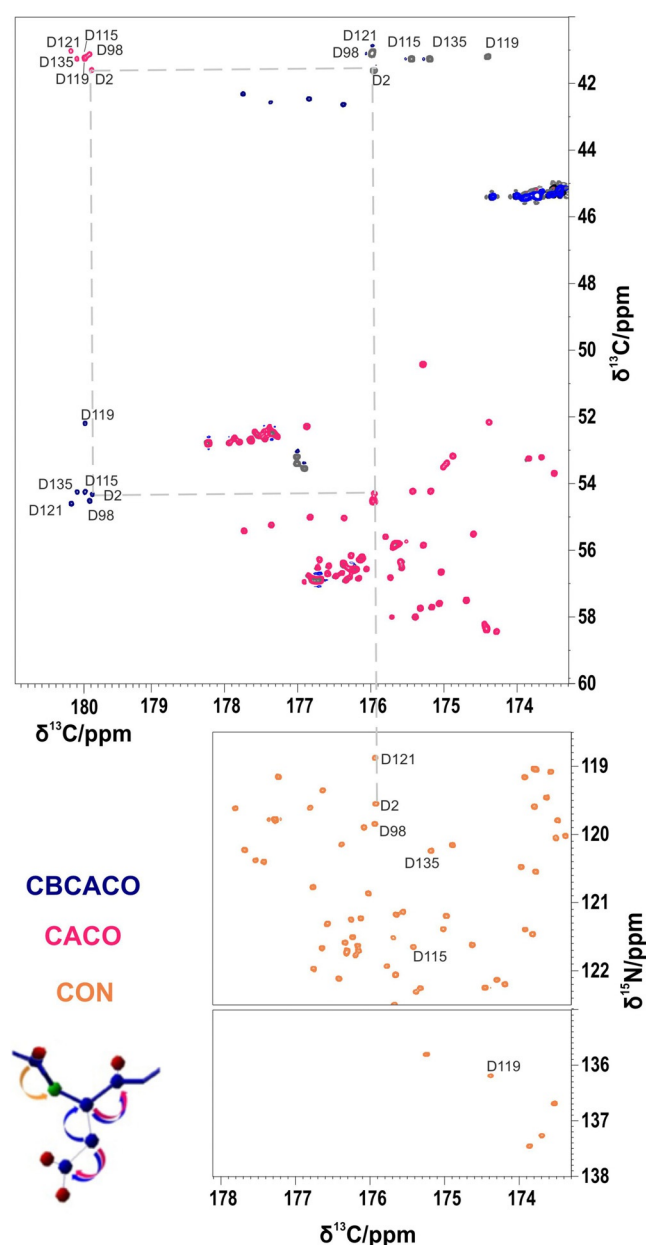

CBCACO

CACO

CON

Figure 1. An illustration of the strategy used to obtain the sequence-specific assignment of the ^{13}C′ resonances of aspartate residues through 2D exclusively heteronuclear NMR experiments. As an example, gray dotted lines indicate the steps followed to assign side-chain resonances of Asp 2. Starting from the carbonyl resonance identified in the CON spectrum (orange), C^α_i and C^β_i are identified in CACO (red) and CBCACO (blue) spectra, superimposed in the Figure, and correlated to C^γ_i through the respective C^β_i-C^γ_i and C^α_i-C^γ_i cross-peaks in a sequence-specific manner.

mission of nervous signals.[39–41] While intracellular Ca^{2+} concentrations are generally very low, microdomains of high Ca^{2+} concentrations are linked to the release of neurotransmitter from presynaptic terminals in all neurons.[26] Having the assignment in hand, it is now possible to "zoom in" on the metal ion coordination sphere and access additional complementary information to that available through HN HSQC experiments.[39]

The set of 2D exclusively heteronuclear NMR experiments, in particular the CON and the CACO, was used to monitor the changes in α-synuclein induced by the presence of Ca²⁺. The chemical shift changes of Asp/Glu residues signals upon addition of Ca²⁺, reported in Figure 2, show that not all of them are affected to the same extent: major changes are observed in the C-terminal region of the protein (110–140), the second part of the so-called acidic region (95–140). As expected, chemical shift changes of side-chain carboxylates are larger with respect to those observed for backbone carbonyl (C′) resonances (Figure S3), reflecting a more direct effect experienced by side-chain nuclear spins upon interaction with calcium ions. No major changes in secondary structural propensity of the backbone were identified upon interaction with calcium ions (Figure S4).

To assess the general applicability of this set of ¹³C detection experiments, the interaction studies with calcium ions were repeated using a sample with an order of magnitude lower concentration of α-synuclein (50 μM). Despite the relatively low sensitivity of ¹³C, the experiments allowed the obtainment of a clear interaction profile (Figure S5); thanks to the inclusion of ¹H as starting polarization source the (H)CACO could be acquired in a few hours (Figures S2 and S5).
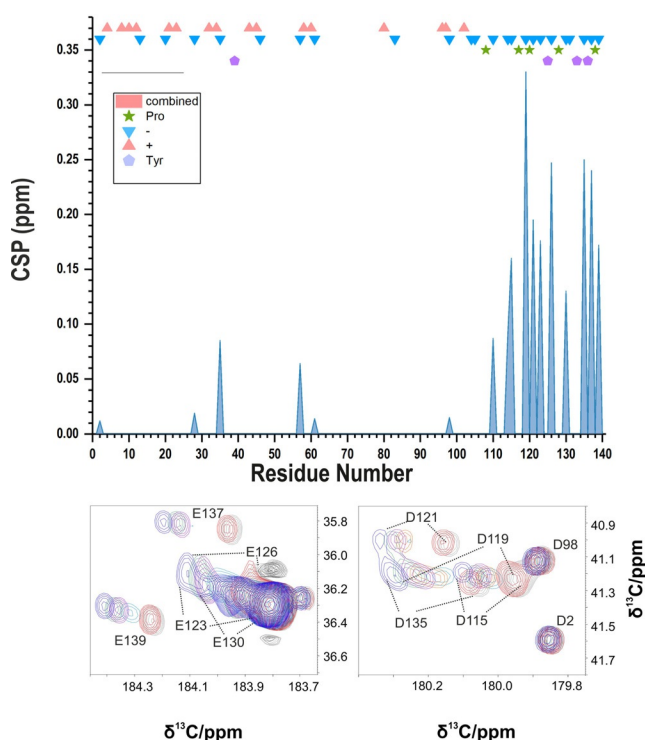
Shifting our attention to backbone nuclear spins by inspection of the combined chemical shift changes of C′ and N chemical shifts,[42] not only direct but also indirect changes derived from the interaction with Ca²⁺ can be monitored (Figure 3). Major perturbations are observed in the final part of the primary sequence (Leu 113, Pro 120, Tyr 125, Met 127, Ser 129, Tyr 136 and Pro 138).

The final part of the polypeptide chain is rich in proline residues with four of the five proline residues of the protein located between residues 117 and 138 (4 out of 22 amino acids in this region). Chemical shift changes of proline residues' signals, that could be monitored through CON spectra (Figure 3), clearly show that two of them, Pro 120 and Pro 138, are significantly perturbed upon addition of Ca²⁺, indicating that they are involved in the interaction of α-synuclein with calcium ions. This may appear surprising since proline does not have metal binding properties. However, these two proline residues are both flanked by two negatively charged amino acids, which all experience significant chemical shift changes for carboxylate resonances. Further inspection of the most pronounced backbone chemical shift changes reveals that two tyrosine residues, which are not so common in IDPs, are also significantly perturbed by Ca²⁺ addition. These observations prompted us to inspect the
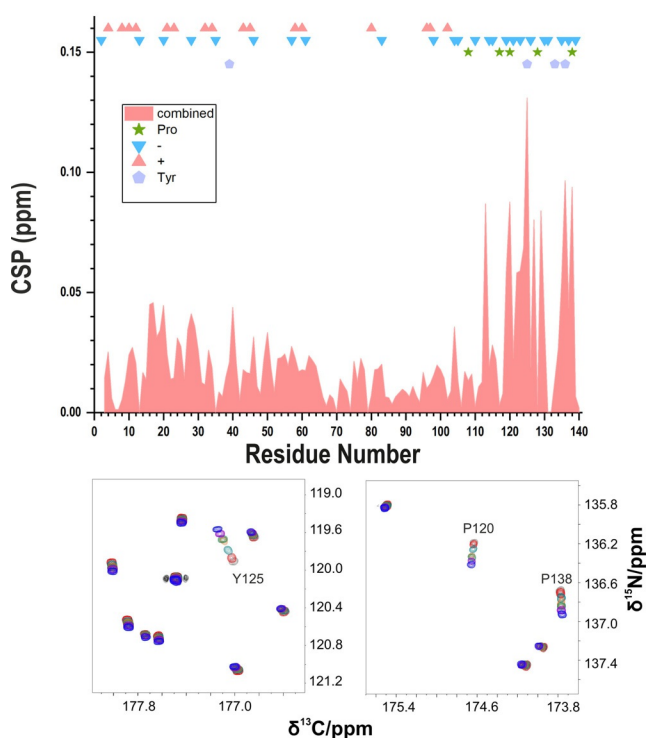

Figure 2. Chemical shift perturbation (difference in absolute value) of aspartate and glutamate side-chain ¹³C resonances upon addition of Ca²⁺. The symbols over the graph depict the distribution of charged, tyrosine and proline residues to evidence the particular composition along the primary sequence: Asp and Glu (blue triangles), Lys (red triangles), Pro (stars) and Tyr (pentagons). The lower panels show two regions of the CACO spectrum with cross-peaks of Asp and Glu side chains and their shifts during the titration. The different extent of the perturbation of Asp and Glu side-chain resonances is evident. Major changes are observed in the C-tail, which is rich in negative charges.

Figure 3. Chemical shift perturbation[42] $\sqrt{0.15\delta(^{15}N_i)^2 + 0.34\delta(^{13}C_i)^2}$ of CON signals upon addition of Ca²⁺. The lower panels show the shift for the two proline residues (Pro 120 and Pro 138 (right)) and for tyrosine 125 (left), the most affected residues during the titration. While the C-terminus is still the most perturbed part, the plot highlights a more indirect effect for the backbone resonances and also reveals an impact on many residues in the N-terminal domain. The titration follows the pattern from blue (α-*syn*:Ca²⁺, 1:0) to purple (α-*syn*:Ca²⁺, 1:16).

positions of proline and tyrosine residues along the primary sequence (schematically depicted in the top of Figures 2 and 3). The results show that the region of the primary sequence of α-synuclein experiencing the most pronounced changes upon Ca^{2+} interaction, that is the final part of the C-terminal region which is very rich in negatively charged amino acids while being depleted of positively charged residues, has also a peculiar abundance of proline and tyrosine residues. The NAC region instead is the one characterized by the smallest chemical shift changes while the N-terminal part of the protein experiences significant variations of backbone chemical shifts. These are less pronounced with respect to those observed for the C-terminal region and are likely to arise in part from an indirect effect of calcium binding, resulting from reduced long range electrostatic interactions between the initial and final part of the protein as observed in other studies.[43,44] It is thus interesting to investigate whether the interaction with Ca^{2+} promotes compaction or decompaction along the primary sequence.

"Spying" chemical exchange of IDPs with water: the DeCON experiment

Exchange of amide protons with the solvent, responsible in our experimental conditions for broadening beyond detection more than half of the signals of amide protons (Figure S6),[45] has been one of the first NMR observables used in the past to identify amide protons protected from solvent exchange by globular protein folds.[46] On the other hand, only a little information is available so far on how solvent exchange is modulated by the properties of IDPs/IDRs. It is thus interesting to investigate this aspect in more detail. A modified variant of the CON was thus designed to reintroduce a dependence on chemical exchange processes with the solvent without perturbing the solvent resonance, still retaining the excellent resolution of CON spectra. The modified pulse sequence (Figure 4A) enables us to create three spin order operator $(4C'_zN_zH_z)$ and to monitor its decorrelation due to chemical exchange, along the lines of a method initially proposed by Skrynnikov and Ernst.[47]

The novel experiment (DeCON) can thus provide information about exchange processes of labile amide protons with the solvent also for residues that escape detection in ^1H-^{15}N-based experiments. Starting from C'_z magnetization (*a*), transverse C'_y coherence is created (*b*) and converted into antiphase coherence $2C'_xN_z$ (*c*). This is then converted into $2C'_zN_y$ (*d*) and allowed to evolve under the effect of the $^1J_{HN}$ coupling to generate $4C'_zN_xH_z$ (*e*). In order to generate this latter operator a band-selective 180° pulse on the amide proton region is used to avoid perturbation of the water resonance. This operator is then converted to the three spin order $4C'_zN_zH_z$ (*f*) and its decay is monitored by introducing a free evolution delay (τ_{decor}). At the end of this delay the three spin order $4C'_zN_zH_z$ is converted to $4C'_zN_yH_z$ (*g*) which is picked up by the second part of the CON after conversion into $2C'_zN_y$ (*h*). It is worth noting that through this approach a dependence on solvent exchange is reintroduced with minimal perturbation of the water resonance avoiding
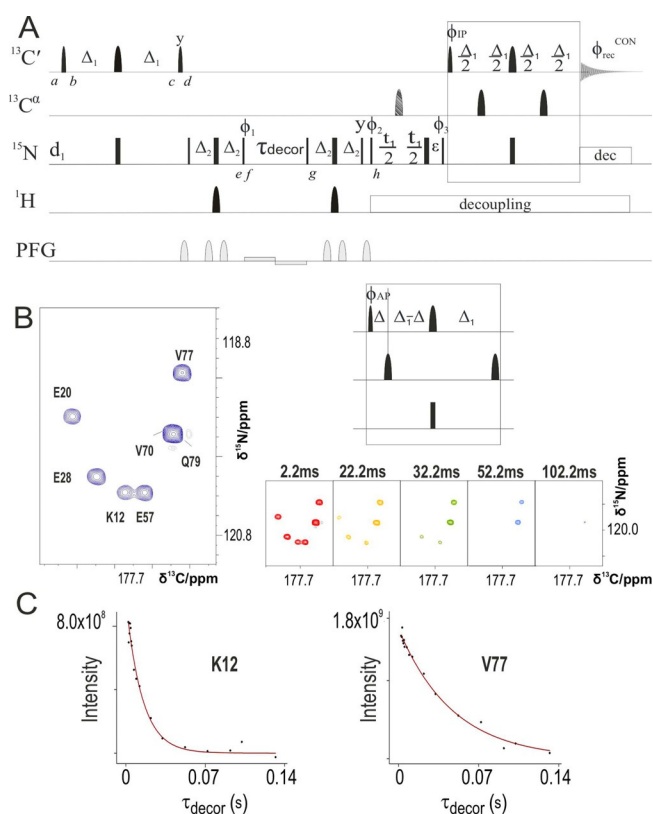

Figure 4. A) DeCON pulse sequence. The following phase cycling was employed: $\phi_1 = 2(y), 2(-y)$; $\phi_2 = x, -x$; $\phi_3 = 4(x), 4(-x)$, $\phi^{IP} = x$; $\phi^{AP} = -y$ and $\phi_{rec} = x, -x, -x, x, -x, x, x, -x$. The length of the delays were: $\Delta = 4.5$ ms $\Delta_1 = 16.6$ ms; $\Delta_2 = 2.7$ ms; $\varepsilon = t_1(0) + p180$ (500 μs). The striped pulse in the middle of the ^{15}N evolution period is an adiabatic chirp pulse that covers the whole ^{13}C spectral region. Virtual decoupling of the C'-C$^\alpha$ coupling was achieved by acquiring both the IP and AP component of the signals for each increment. The strength of the smoothed square shape gradients are: 50%, 19%, 19%, 25%, 25%, 70%; the strength of the weak bipolar gradient is 1%. Quadrature detection in the indirect dimension was obtained with the STATES-TPPI approach incrementing phase ϕ_2. B) A portion of the 2D DeCON spectrum is shown on the left with the assignment of the cross-peaks; several spectra acquired as a function of τ_{decor} are shown on the right. C) The intensities (arbitrary units) of two of these cross-peaks are reported as a function of τ_{decor}

radiation damping effects. As an example, a region of the spectrum obtained with this novel DeCON experiment is shown in Figure 4B as a function of τ_{decor}, the time interval in which the three spin order $4C'_zN_zH_z$ is allowed to evolve: while the signal of Val 77 is still observable with τ_{decor} = 52.2 ms, one of the Lys 12 signals disappears with τ_{decor} = 22.2 ms. The intensities of cross-peaks can be integrated in the series of spectra acquired with a different τ_{decor} and can be fit to a mono-exponential decay $(I_{zzz}(\tau_{decor}) = I_0 e^{-(k_{zzz}\tau_{decor})}$, Figure 4C).

It is interesting to compare the results obtained through the DeCON experiment proposed here with the ones obtained through the initially proposed ^1H detected variant[47] (HN-Decor experiment). The agreement between the data measured through the two different experiments is quite good for the residues that could be detected in both experiments

(Figure S7). The DeCON however provides information about a larger number of residues with respect to the ^{1}H detected variant. This is in part due to the improved resolution derived from the superior chemical shift dispersion of the C'_{i-1}-N_i correlations with respect to the H_i-N_i correlations, and in part to the different magnetization transfer pathway minimizing perturbation of ^{1}H magnetization (in the HN coherence transfer pathway the proton magnetization is transverse both during the two INEPT steps and the acquisition, in the DeCON the proton magnetization is maintained along the z-axis). These properties of the DeCON experiment allow us to monitor a larger number of residues and to extend the range of k_{zzz} values that can be measured with respect to the ^{1}H detected variant. The minor contribution of longitudinal relaxation to the observed decay was evaluated investigating the decay of the $2C'_zN_z$ operator (Figure S8). Finally, a three-dimensional variant of the DeCON experiment was designed to further increase the resolution of the experiment in a third dimension exploiting C^α chemical shifts, opening the possibility of studying IDPs of increasing size (Figure S9).

The k_{zzz} values determined through the DeCON experiment are reported as a function of the residue number in Figure S10. The residues in the initial part of the polypeptide chain show significantly high values which are however quite scattered along the primary sequence, an effect largely due to the type of amino acid as indicated in Figure S10. The C-terminal region (110–140) shows significantly reduced exchange processes, in agreement with previous observations attributed to the effect of the high local negative potential.[9] With increasing temperature or pH (or both) the k_{zzz} values increase while the trend along the protein primary sequence is maintained (data not shown).

Upon addition of Ca^{2+} to the α-synuclein sample the k_{zzz} values determined through the DeCON experiment show a global enhancement along the primary sequence, while maintaining the general trend as shown in Figure S11. The effect appears more relevant for the residues in the terminal parts; the ratio between k_{zzz} of the bound and the unbound forms is shown in Figure 5. In the central zone (residues 40–100), the average value of k_{zzz}(α-synCa)/k_{zzz}(α-syn) = 1.10, while several residues in the terminal parts (1–39 and 101–140) present a higher ratio. The residues that experience the higher boost (over ×1.9 times respect to the unbound form) are Ala 18, Ala 30, Glu 115, Asp 119, Asp 121, Asn 122, Glu 123, Ala 124, Tyr 125, Ser 129, Tyr 133, Gln 134, Asp 135 and Tyr 136. The global increase observed in the exchange rates could be due in part to an increase in ionic strength during the titration with $CaCl_2$. In contrast, the very strong and localized effect in the terminal domains should be related to different reasons, such as reduction of the electrostatic potential in the C-terminal region and disruption of the electrostatic interactions between the N-terminal and C-terminal parts of the polypeptide chain. On the other hand the present data show no evidence of formation of a more compact state in which solvent exchange is precluded upon interaction with calcium ions.
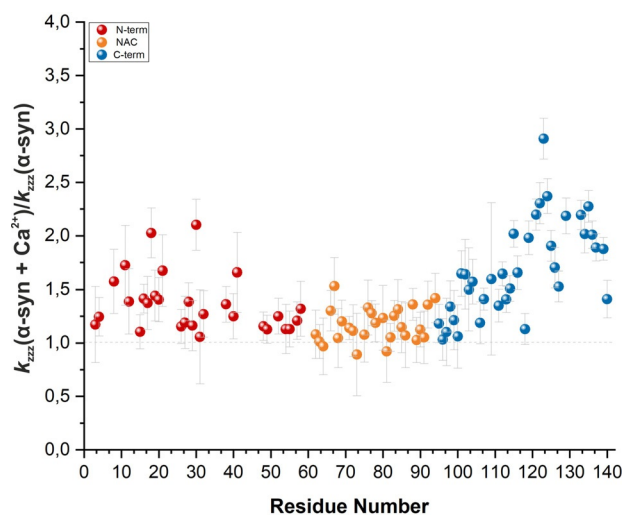

Figure 5. Ratio of the k_{zzz} values obtained from the DeCON experiments before and after addition of Ca^{2+}. The plot evidences the different effects in the increment for the three α-synuclein regions: while NAC (yellow) maintains a homogeneous trend, C-terminus (blue) shows the major boost, in line with the defined binding region. However, it is possible to see an increment also for some scattered residues in the N-terminal part (red).

Ca^{2+} sensing by α-synuclein: new insights

The high number of negatively charged amino acids in the final part of the primary sequence of α-synuclein, in combination with the disordered nature of this protein that leaves this part of the backbone largely solvent-exposed and easily accessible, provides a strong electrostatic negative potential that is likely to have an important role for its function, in particular in mediating interactions with positively charged entities (ions, small molecules, proteins, etc.). This is likely to create the initial driving force, sensed at quite long distance, for the interaction with Ca^{2+}.[35] The negatively charged functional groups of amino acid side chains, such as carboxylate groups of aspartate and glutamate residues (COO^-), in principle all have the potential to interact with positively charged metal ions. The disordered nature of the polypeptide that leaves COO^- groups largely exposed to the solvent would suggest an unspecific effect, with all COO^- sharing similar interaction properties. Instead, we find very specific differential effects for the COO^- groups in the different parts of the polypeptide chain. The sequence context thus has an important role in mediating interactions with Ca^{2+} even in the case of IDPs. The possibility to directly observe perturbations sensed by COO^- groups through ^{13}C detection experiments allows us to zoom in on the interaction site and identify the amino acids that are the most perturbed by calcium addition. Interestingly the largest perturbations are found in the C-terminal tract for the following residues: Asp 119, Asp 121, Glu 123, Glu 126, Asp 135, Glu 137 and Glu 139. These residues belong to an extended region of the polypeptide chain (119–139, 21 amino acids long) showing that Ca^{2+} already has a strong preference for a subset of the COO^- groups in the C-terminal region in which α-synuclein is usually subdivided (95–140). Looking in more detail, two

regions, which are quite far from each other, can be identified: Asp 119–Glu 126 and Asp 135–Glu 139. These two distinct regions share very similar patterns: 1) negatively charged amino acids are close in the primary sequence but not contiguous, 2) in two cases amino acids in between negatively charged amino acids are prolines, and 3) in two cases glutamate is preceded by tyrosine. Therefore the signature in terms of amino acidic composition of these regions strongly perturbed by the addition of calcium ions is very characteristic. Specific patterns can thus be identified that are likely to play an important role in modulating calcium ion interactions: a pair of negatively charged amino acids (Asp or Glu) separated by a proline (Asp 119–Pro 120–Asp 121 and Glu 137–Pro 138–Glu 139), tyrosine-glutamate motifs (Tyr 125–Glu 126 and Tyr 136–Glu 137).

The role of a proline in between two negatively charged amino acids could thus be important to reduce local mobility and favor the proper relative orientation of negatively charged side chains for calcium binding (Figure 6). Tyrosine residues are very bulky amino acids with aromatic side chains rich in π electron density, two properties that could play a relevant role in reducing local motions and favoring interactions of highly flexible protein regions with Ca^{2+}, in particular if followed by an acidic residue providing a COO^- group. These could be key elements of specific motifs to modulate Ca^{2+} sensing in highly flexible protein tracts. The question of whether a stable complex is formed or an equilibrium between different local binding sites with similar affinities is established remains. On one hand the flexibility of the polypeptide chain provides to the system the necessary degrees of freedom to fold around a unique metal binding site, on the other hand the entropic penalty associated to folding a tract of 20 amino acids is expected to be much higher than that of multiple sites with comparable affinity in equilibrium, each of them comprising 6–8 amino acids.

It is thus interesting to zoom out and inspect chemical shift changes observed for backbone nuclear spins in this region. The major changes are observed for residues 119–129 and for residues 134–139. Interestingly the two proline residues in the new motif identified from side-chain chemical shifts (Pro 120 and Pro 138, both flanked by negatively charged amino acids) are the ones that show the largest

chemical shifts changes (Figure 3), confirming their important role in the interaction with Ca^{2+}. Tyrosine 125 also shows pronounced changes upon interaction (Figure 3) as well as Tyr 136 (data not shown). Chemical shift changes, although significant, do not indicate the formation of a defined folded state. The overall properties of this tract are still in line with a highly flexible state. Exchange properties of amide protons with the solvent, as monitored through the novel DeCON experiment, show an increase in the decorrelation upon addition of Ca^{2+} which shows that the backbone is still largely accessible to solvent exchange, definitely far from forming a protected pocket in which solvent exchange is precluded. Therefore the interaction of α-synuclein with Ca^{2+} appears more in line with a fuzzy interaction in which flexibility and disorder is maintained also upon interaction. The strong electrostatic potential of the C-terminal tail could play the initial important driving force, sensed also at long range, for the interaction with calcium ions; the identified motifs in the primary sequence could act as nucleation sites for the interaction. A number of conformations would then be easily accessible to engage other Asp/Glu residues in the interaction with calcium ions.

The interaction of α-synuclein with Ca^{2+} is likely to disrupt the interaction of the C-terminal region with the N-terminal region, rich of lysine residues. This region adopts a helical conformation when bound to membranes[12–14] and was proposed to form long range interactions at the origin of a compact state of α-synuclein populated in solution.[10,11,48,50] Our data confirm that chemical shift changes are observed for residues in the N-terminal region which could be explained, at least in part, by disruption of long range interactions. Indeed, most of the COO^- groups of aspartate and glutamate side chains in the N-terminal region only show modest chemical shift changes, much less than those observed in the C-terminal region. In addition, changes in solvent exchange properties are observed through DeCON for the initial part of the polypeptide chain. These could result in part by an increased solvent accessibility resulting from loss of the compact conformation. However, we cannot rule out the possibility of the occurrence of other intermolecular effects. A detailed investigation of the long range effects of Ca^{2+} addition would require additional experiments, for example exploiting paramagnetic relaxation enhancements induced by the presence of a paramagnetic tag, which might take advantage of ^{13}C NMR detection experiments.[51]

Metal binding sites of globular, folded proteins have been extensively investigated revealing their key role in structure function relationships. The interactions of metal ions with highly flexible protein regions instead are only beginning to be investigated in detail to understand their structural and dynamic properties and their impact on protein function. The experiments proposed here provide a useful tool to investigate the interactions of flexible protein tracts with metal ions at high resolution. The example of the interaction of α-synuclein with Ca^{2+} reveals specific motifs in the protein primary sequence providing a glimpse on the wide versatility through which proteins modulate interactions with calcium ions also through high flexibility and disorder. Very few of these disordered motifs have been investigated at high
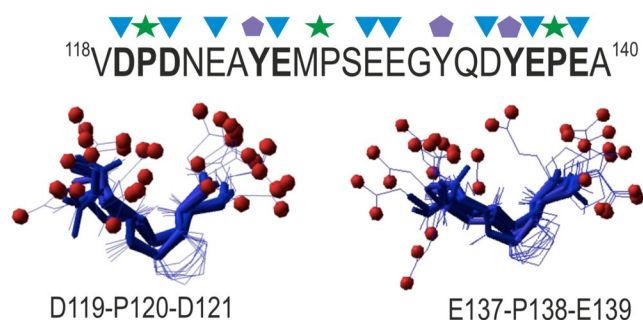

Figure 6. Structural models of the DPD and EPE motifs identified in α-synuclein as strongly perturbed as a result of Ca^{2+} concentration jumps. The structural conformers are calculated through Flexible Meccano[48] without imposing any constraints. The Figure was obtained using MOLMOL.[49]

resolution and many more could be studied in detail with the tools proposed here. The characteristic features identified in α-synuclein might also be useful as input for bioinformatics tools to search for similar Ca^{2+} binding patterns in disordered proteins.

α-synuclein has also been shown to interact with other metal ions.[36–38,52] Among them Cu^{II}, Fe^{II}, Co^{II}, Ni^{II}, Mn^{II}, and several lanthanide metal ions[38,53,54] many of which are paramagnetic. The set of experiments proposed here might be useful to provide additional insights on the mode of interaction. As an example we tested Mn^{II}, which provides very strong paramagnetic effects deriving from the high number of unpaired electrons combined with a relatively long electronic relaxation time.[55] Previous NMR investigations revealed that Mn^{II} interacts with residues in the C-terminal region of α-synuclein, in a very similar way to what observed for Ca^{2+}.[38] A sub-stoichiometric concentration of Mn^{II} (1/100 respect to the protein concentration) indeed shows that first carboxylate groups to be perturbed by the interaction are the same ones identified in the interaction with Ca^{2+} (Figure 7). Further additions of Mn^{II} allow to progressively zoom out and identify the first backbone resonances to be perturbed as well as the region mainly affected.
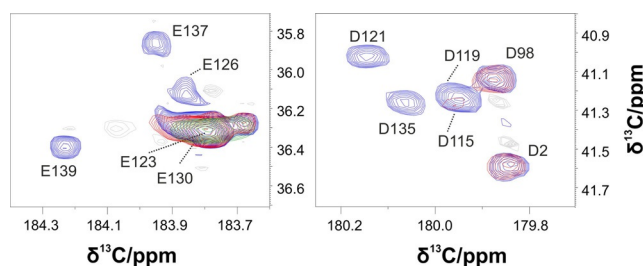

Figure 7. The panels show two regions of the CACO spectrum with cross-peaks of Asp and Glu side chains and their shifts upon Mn^{2+} addition. The Figure shows that the first carboxylate groups to be perturbed by the interaction with Mn^{2+} are the same ones identified in the interaction with Ca^{2+}.

Conclusion

The improved set of 2D exclusively heteronuclear NMR experiments based on carbonyl direct detection enabled us to resolve the signals of COO- groups of α-synuclein amino acid side chains and to monitor local solvent exposure. These experiments allowed us to zoom in on the metal ion coordination sphere, revealing novel motifs involved in the interaction with calcium ions. This represents just one example of the key role played by solvent-exposed side chains in modulating the biological function of highly flexible protein tracts. Post-translational modifications, which often involve solvent-exposed amino acid side chains, introduce another layer of complexity in modulating protein function that can be studied through the approach presented herein. The proposed experiments can thus become a tool of general interest to characterize the properties of IDPs/IDRs in physiologically relevant conditions that have not been studied

so far, thereby significantly expanding our knowledge on how protein function is modulated by disorder and flexibility.

Conflict of interest

The authors declare no conflict of interest.

[1] A. K. Dunker, M. M. Babu, E. Barbar, M. Blackledge, S. E. Bondos, Z. Dosztányi, H. J. Dyson, J. Forman-Kay, M. Fuxreiter, J. Gsponer, K.-H. Han, D. T. Jones, S. Longhi, S. J. Metallo, K. Nishikawa, R. Nussinov, Z. Obradovic, R. V. Pappu, B. Rost, P. Selenko, V. Subramaniam, J. L. Sussman, P. Tompa, V. N. Uversky, *Intrinsically Disord. Proteins* **2013**, *1*, e24157.

[2] R. van der Lee, M. Buljan, B. Lang, R. J. Weatheritt, G. W. Daughdrill, A. K. Dunker, M. Fuxreiter, J. Gough, J. Gsponer, D. T. Jones, P. M. Kim, R. W. Kriwacki, C. J. Oldfield, R. V. Pappu, P. Tompa, V. N. Uversky, P. E. Wright, M. M. Babu, *Chem. Rev.* **2014**, *114*, 6589–6631.

[3] J. Habchi, P. Tompa, S. Longhi, V. N. Uversky, *Chem. Rev.* **2014**, *114*, 6561–6588.

[4] M. Arbesú, M. Pons, *Arch. Biochem. Biophys.* **2019**, *677*, 108161.

[5] L. Geist, M. A. Henen, S. Haiderer, T. C. Schwarz, D. Kurzbach, A. Zawadzka-Kazimierczuk, S. Saxena, S. Zerko, W. Koźmiński, D. Hinderberger, R. Konrat, *Protein Sci.* **2013**, *22*, 1196–1205.

[6] F. Theillet, A. Binolfi, T. Frembgen-Kesner, K. Hingorani, M. Sarkar, C. Kyne, C. Li, P. B. Crowley, L. Gierasch, G. J. Pielak, A. H. Elcock, A. Gershenson, P. Selenko, *Chem. Rev.* **2014**, *114*, 6661–6714.

[7] *Intrinsically Disordered Proteins Studied by NMR Spectroscopy* (Eds.: I. C. Felli, R. Pierattelli), Springer, Heidelberg, **2015**.

[8] J. H. Ardenkjaer-Larsen, G. S. Boebinger, A. Comment, S. Duckett, A. S. Edison, F. Engelke, C. Griesinger, R. G. Griffin, C. Hilty, H. Maeda, G. Parigi, T. Prisner, E. Ravera, J. Van Bentum, S. Vega, A. Webb, C. Luchinat, H. Schwalbe, L. Frydman, *Angew. Chem. Int. Ed.* **2015**, *54*, 9162–9185; *Angew. Chem.* **2015**, *127*, 9292–9317.

[9] R. L. Croke, C. O. Sallum, E. Watson, E. D. Watt, A. T. Alexandrescu, *Protein Sci.* **2008**, *17*, 1434–1445.

[10] M. M. Dedmon, K. Lindorff-Larsen, J. Christodoulou, M. Vendruscolo, C. M. Dobson, *J. Am. Chem. Soc.* **2005**, *127*, 476–477.

[11] C. W. Bertoncini, Y. Jung, C. O. Fernández, W. Hoyer, C. Griesinger, T. M. Jovin, M. Zweckstetter, *Proc. Natl. Acad. Sci. USA* **2005**, *102*, 1430–1435.

[12] S. Chandra, X. Chen, J. Rizo, R. Jahn, T. C. Südhof, *J. Biol. Chem.* **2003**, *278*, 15313–15318.

[13] T. S. Ulmer, A. Bax, N. B. Cole, R. L. Nussbaum, *J. Biol. Chem.* **2005**, *280*, 9595–9603.

[14] C. R. Bodner, C. M. Dobson, A. Bax, *J. Mol. Biol.* **2009**, *390*, 775–790.

[15] G. Fusco, T. Pape, A. D. Stephens, P. Mahou, A. R. Costa, C. F. Kaminski, G. S. Kaminski Schierle, M. Vendruscolo, G. Veglia, C. M. Dobson, A. De Simone, *Nat. Commun.* **2016**, *7*, 12563.

[16] M. D. Tuttle, G. Comellas, A. J. Nieuwkoop, D. J. Covell, D. A. Berthold, K. D. Kloepper, J. M. Courtney, J. K. Kim, A. M. Barclay, A. Kendall, W. Wan, G. Stubbs, C. D. Schwieters, V. M. Y. Lee, J. M. George, C. M. Rienstra, *Nat. Struct. Mol. Biol.* **2016**, *23*, 409–415.

[17] A. D. Stephens, M. Zacharopoulou, G. S. Kaminski Schierle, *Trends Biochem. Sci.* **2019**, *44*, 453–466.

[18] V. N. Uversky, *J. Biomol. Struct. Dyn.* **2003**, *21*, 211–234.

[19] W. Bermel, I. Bertini, I. C. Felli, R. Peruzzini, R. Pierattelli, *ChemPhysChem* **2010**, *11*, 689–695.

[20] I. Bertini, I. C. Felli, L. Gonnelli, M. V. Vasantha Kumar, R. Pierattelli, *Angew. Chem. Int. Ed.* **2011**, *50*, 2339–2341; *Angew. Chem.* **2011**, *123*, 2387–2389.

[21] S. Gil, T. Hošek, Z. Solyom, R. Kümmerle, B. Brutscher, R. Pierattelli, I. C. Felli, *Angew. Chem. Int. Ed.* **2013**, *52*, 11808–11812; *Angew. Chem.* **2013**, *125*, 12024–12028.

[22] J. Lopez, P. Ahuja, M. Gerard, J. M. Wieruszeski, G. Lippens, *J. Magn. Reson.* **2013**, *236*, 1–6.

[23] I. C. Felli, L. Gonnelli, R. Pierattelli, *Nat. Protoc.* **2014**, *9*, 2005–2016.

[24] E. C. Cook, G. A. Usher, S. A. Showalter, *Methods Enzymol.* **2018**, *611*, 81–100.

[25] A. Alik, C. Bouguechtouli, M. Julien, W. Bermel, R. Ghouil, S. Zinn-Justin, F. X. Theillet, *Angew. Chem. Int. Ed.* **2020**, *59*, 10411–10415; *Angew. Chem.* **2020**, *132*, 10497–10501.

[26] R. Llinás, M. Sugimori, R. B. Silver, *Science* **1992**, *256*, 677–679.

[27] R. Schneggenburger, E. Neher, *Nature* **2000**, *406*, 889–893.

[28] H. J. Lee, E. J. Bae, S. J. Lee, *Nat. Rev. Neurol.* **2014**, *10*, 92–98.

[29] W. Bermel, I. Bertini, L. Duma, I. C. Felli, L. Emsley, R. Pierattelli, P. R. Vasos, *Angew. Chem. Int. Ed.* **2005**, *44*, 3089–3092; *Angew. Chem.* **2005**, *117*, 3149–3152.

[30] W. Bermel, I. Bertini, I. C. Felli, M. Piccioli, R. Pierattelli, *Prog. Nucl. Magn. Reson. Spectrosc.* **2006**, *48*, 25–45.

[31] L. E. Kay, M. Ikura, R. Tschudin, A. Bax, *J. Magn. Reson.* **1990**, *89*, 496–514.

[32] M. Sattler, C. Schleucher, J. Griesinger, *Prog. Nucl. Magn. Reson. Spectrosc.* **1999**, *34*, 93–158.

[33] A. Bax, *J. Magn. Reson.* **2011**, *213*, 442–445.

[34] C. O. Fernández, W. Hoyer, M. Zweckstetter, E. A. Jares-Erijman, V. Subramaniam, C. Griesinger, T. M. Jovin, *EMBO J.* **2004**, *23*, 2039–2046.

[35] M. S. Nielsen, H. Vorum, E. Lindersson, P. H. Jensen, *J. Biol. Chem.* **2001**, *276*, 22680–22684.

[36] R. M. Rasia, C. W. Bertoncini, D. Marsh, W. Hoyer, D. Cherny, M. Zweckstetter, C. Griesinger, T. M. Jovin, C. O. Fernández, *Proc. Natl. Acad. Sci. USA* **2005**, *102*, 4294–4299.

[37] Y. H. Sung, C. Rospigliosi, D. Eliezer, *Biochim. Biophys. Acta Proteins Proteomics* **2006**, *1764*, 5–12.

[38] A. Binolfi, R. M. Rasia, C. W. Bertoncini, M. Ceolin, M. Zweckstetter, C. Griesinger, T. M. Jovin, C. O. Fernández, *J. Am. Chem. Soc.* **2006**, *128*, 9893–9901.

[39] J. Lautenschläger, A. D. Stephens, G. Fusco, F. Ströhl, N. Curry, M. Zacharopoulou, C. H. Michel, R. Laine, N. Nespovitaya, M. Fantham, D. Pinotsi, W. Zago, P. Fraser, A. Tandon, P. St George-Hyslop, E. Rees, J. J. Phillips, A. De Simone, C. F. Kaminski, G. S. K. Schierle, *Nat. Commun.* **2018**, *9*, 712.

[40] A. Rcom-H'cheo-Gauthier, J. Goodwin, D. L. Pountney, *Biomolecules* **2014**, *4*, 795–811.

[41] M. R. Post, O. J. Lieberman, E. V. Mosharov, *Front. Neurosci.* **2018**, *12*, 161.

[42] M. P. Williamson, *Prog. Nucl. Magn. Reson. Spectrosc.* **2013**, *73*, 1–16.

[43] Y. Yoshimura, M. A. Holmberg, P. Kukic, C. B. Andersen, A. Mata-Cabana, S. Fabio Falsone, M. Vendruscolo, E. A. A. Nollen, F. A. A. Mulder, *J. Biol. Chem.* **2017**, *292*, 8269–8278.

[44] A. Beier, T. C. Schwarz, D. Kurzbach, G. Platzer, F. Tribuzio, R. Konrat, *J. Mol. Biol.* **2018**, *430*, 2439–2452.

[45] M. Schiavina, M. G. Murrali, L. Pontoriero, V. Sainati, R. Kümmerle, W. Bermel, R. Pierattelli, I. C. Felli, *Biophys. J.* **2019**, *117*, 46–55.

[46] Y. Bai, J. S. Milne, L. Mayne, S. W. Englander, T. R. Sosnick, L. Mayne, S. W. Englander, J. S. Milne, L. Mayne, S. W. Englander, *Proteins Struct. Funct. Genet.* **1993**, *17*, 75–86.

[47] N. R. Skrynnikov, R. R. Ernst, *J. Magn. Reson.* **1999**, *137*, 276–280.

[48] V. Ozenne, F. Bauer, L. Salmon, J. R. Huang, M. R. Jensen, S. Segard, P. Bernadó, C. Charavay, M. Blackledge, *Bioinformatics* **2012**, *28*, 1463–1470.

[49] R. Koradi, M. Billeter, K. Wüthrich, *J. Mol. Graph.* **1996**, *14*, 51–55.

[50] M. K. Janowska, J. Baum in *Methods in Molecular Biology* (Ed.: D. Eliezer), Springer New York, New York, **2016**, pp. 45–53.

[51] B. Mateos, R. Konrat, R. Pierattelli, I. C. Felli, *ChemBioChem* **2019**, *20*, 335–339.

[52] A. Santner, V. N. Uversky, *Metallomics* **2010**, *2*, 378–392.

[53] V. N. Uversky, J. Li, A. L. Fink, *J. Biol. Chem.* **2001**, *276*, 44284–44296.

[54] J. Bai, Z. Zhang, M. Liu, C. Li, *BMC Biophys.* **2016**, *9*, 1.

[55] I. Bertini, C. Luchinat, G. Parigi, E. Ravera, *NMR of Paramagnetic Molecules*, Elsevier, Amsterdam, **2017**.